

NMR Detection with an Atomic Magnetometer

I. M. Savukov and M. V. Romalis

Department of Physics, Princeton University, Princeton, New Jersey 08544, USA

(Received 13 October 2004; published 29 March 2005)

We demonstrate detection of NMR signals using a noncryogenic atomic magnetometer and describe several novel applications of this technique. A nuclear spin-precession signal from water is detected using a spin-exchange-relaxation-free potassium magnetometer. We also demonstrate detection of less than 10^{13} ^{129}Xe atoms whose NMR signal is enhanced by a factor of 540 due to Fermi-contact interaction with K atoms. The possibility of using a multichannel atomic magnetometer for fast 3D magnetic resonance imaging is also discussed.

DOI: 10.1103/PhysRevLett.94.123001

PACS numbers: 33.25.+k, 82.56.-b, 83.85.Fg, 87.61.-c

Nuclear magnetic resonance signals are usually detected with inductive rf pickup coils. A high magnetic field, typically produced by a superconducting magnet, improves the signal strength approximately as B^2 and increases the ability to resolve NMR chemical shifts. In applications that do not require chemical shift information it is possible to avoid using a large magnetic field by utilizing a magnetometer instead of an inductive pickup coil, making the signal strength proportional only to the first power of B [1,2]. It is even possible to completely eliminate the dependence of the signal strength on the magnetic field by utilizing hyperpolarized nuclei, such as ^{129}Xe polarized by spin-exchange optical pumping [3] or protons polarized by spin polarization induced nuclear Overhauser effect [4]. However, nearly all previous demonstrations of NMR detection with a magnetometer relied on SQUID sensors that operate at cryogenic temperatures and impede applications of NMR and MRI in portable, maintenance-free systems.

In this Letter we demonstrate NMR detection using a noncryogenic atomic magnetometer and describe several novel applications based on its unique properties. Recent advances in atomic magnetometry [5], in particular demonstration of a spin-exchange-relaxation-free (SERF) magnetometer [6], have allowed alkali-metal magnetometers to exceed the sensitivity of low-temperature SQUID detectors [7]. Here we demonstrate first detection of NMR spin-precession signals from a thermally polarized water sample with an atomic magnetometer. Previous NMR measurements using atomic magnetometers have only detected the static magnetization of hyperpolarized gases [8–10]. In a separate experiment, we investigate a method for increasing the NMR sensitivity by allowing the nuclei to occupy the same volume as the active atoms of the magnetometer, which increases the NMR signal by a large factor due to the Fermi-contact interaction between the alkali-metal valence electrons and the nuclear spins [11,12]. We detect a signal from 2×10^{13} ^{129}Xe atoms with a signal-to-noise ratio of 10 and a bandwidth of 10 Hz without averaging. Hyperpolarized ^{129}Xe is widely used for MRI [13], as a biosensor [14,15], and for remote NMR detection [16]. For compari-

son, detection of hyperpolarized ^{129}Xe NMR with traditional pickup coils has been demonstrated at a level of 10^{14} spins [17], while micro-coils have been used to detect NMR signals from 3×10^{12} thermally polarized protons [18,19], using some averaging in both cases. Magnetic resonance force microscopy has achieved sensitivity of 7×10^8 ^{71}Ga nuclear spins at cryogenic temperatures [20].

Simple multichannel operation of atomic magnetometers with no inductive coupling between channels may also lead to new MRI techniques. We propose a novel MRI method that allows reconstruction of a complete 3D image from a single free induction decay (FID) signal in the presence of a constant magnetic field gradient by relying on multichannel magnetic field measurements.

Atomic magnetometers operate by measuring the precession of electron spins in a magnetic field, usually using an alkali-metal vapor. The sensitivity of the magnetometer is determined by the number of atoms in the active volume and their transverse spin relaxation time. Atomic collisions usually limit the transverse spin relaxation time, particularly at high alkali-metal density. As was first shown in [21], the dominant relaxation mechanism due to spin-exchange collisions can be eliminated by operating in a very low magnetic field with a high alkali-metal density. Such a spin-exchange relaxation-free (SERF) magnetometer has achieved magnetic field sensitivity of $0.5 \text{ fT}/\text{Hz}^{1/2}$ using an active volume of 0.3 cm^3 [7]. The small active volume is important for obtaining a short effective distance between the magnetometer and the NMR sample. The magnetometer apparatus is described in detail in [6,7]. Briefly, it consists of a glass cell containing K vapor and a high pressure buffer gas to slow the diffusion of atoms across the cell. An optical pumping laser spin-polarizes the atoms while an orthogonal probe laser detects their precession in the magnetic field. Because of slow K diffusion, a single probe laser expanded to fill the whole cell can be used to simultaneously measure the magnetic field in multiple points by imaging it on a multichannel photo detector. In this arrangement most elements of the magnetometer are common, allowing one to construct an inexpensive system

with hundreds or even thousands of channels. One challenge for using an atomic magnetometer for NMR detection is the need to match the resonance frequencies of the electron and nuclear spins whose gyromagnetic ratios are different by a factor of 100–1000. If the atomic magnetometer is used to detect the magnetic field from a separate sample of nuclear spins, one can use a solenoid to create different magnetic fields for the two regions as was recently demonstrated in [10]. If the nuclear spins are directly interacting with the atomic magnetometer, one can use these interactions to match the two resonance frequencies [22].

The experimental arrangement for detection of water NMR is shown in Fig. 1(a). To obtain independent control of the magnetic fields experienced by the protons and the K magnetometer, the water sample is contained in a solenoid that determines the NMR frequency, $\omega_p = \gamma_p B_{\text{sol}} \approx 2\pi \times 20$ Hz, where γ_p is proton's gyromagnetic ratio. The magnetic flux produced by the solenoid is returned through the magnetic shields, so the external field is a factor of 1000 smaller than the internal field. In previous experiments designed to detect NMR with SQUIDS in a very low

magnetic field, the thermal polarization was increased by using a large prepolarizing field [1]. To avoid magnetization of our magnetic shields, we instead used a flow system where the water is prepolarized by a permanent magnet outside of the shields. The K cell is heated to 180°C in a double-wall oven made from thin G7 sheets. Microporous thermal insulation is used to insulate the oven, keeping the total distance between the K cell and the room-temperature surface to about 1 cm. Magnetometer coils inside the shields are used to zero the magnetic field at the K cell to achieve the maximum sensitivity of the SERF magnetometer. One coil is also used to generate a $\pi/2$ pulse to tip the proton spins. The transverse relaxation time of K spins is much shorter than that of protons in water, so the transient signal of the magnetometer decays faster than the water spin-precession signal. A single-shot water NMR signal is shown in Fig. 1(b), and its fast Fourier transform (FFT) is shown in Fig. 1(c). The FFT shows a single peak at the expected proton frequency with a S/N of greater than 10. The S/N is comparable to or better than those obtained with SQUID magnetometers [1].

Another unique aspect of alkali-metal magnetometers is their ability to interact directly with the nuclei of interest. For noble gases the Fermi-contact interaction results in a large enhancement of the usual dipolar field. For a spherical cell, the effective field experienced by the K atoms is given by

$$B_K = \frac{8\pi}{3} \kappa_0 M, \quad (1)$$

where M is the nuclear magnetization [12] and κ_0 ranges from 6 for ^3He [23] to about 600 for ^{129}Xe [24]. The magnetization of K atoms M_K also creates an effective field experienced by the noble gas nuclear spins,

$$B_{\text{Xe}} = \frac{8\pi}{3} \kappa_0 M_K = \frac{8\pi}{3} \kappa_0 g_s \mu_B P_K [\text{K}], \quad (2)$$

where g_s is the electron's g factor, μ_B is the Bohr magneton, and P_K is the potassium polarization. In a high-density alkali-metal vapor this field causes ^{129}Xe atoms to precess at a frequency of a few Hz while K atoms remain in a nearly zero field.

In Fig. 2(a) we illustrate the basic experimental arrangement. A small concentration of ^{129}Xe atoms (740 μTorr of ^{129}Xe enriched to 80%) is added to the magnetometer cell. ^{129}Xe is polarized parallel to the pump beam by spin-exchange collisions with K atoms. To tip the ^{129}Xe spins, a static transverse magnetic field B_x of 1 mG is turned on for about 200 msec. The field causes K atoms to depolarize and ^{129}Xe atoms to precess by $\pi/2$. After the field is turned off, K atoms are quickly repolarized and ^{129}Xe spins precess around the field B_{Xe} . Their transverse oscillating magnetization generates the field B_K which is detected by the magnetometer.

Figure 2(b) shows the spin-precession signal of ^{129}Xe . The data are well described by an exponentially decaying

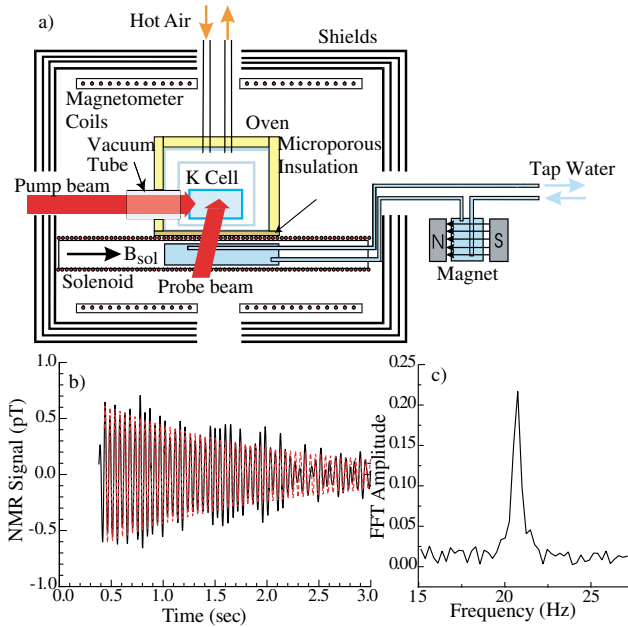


FIG. 1 (color online). Water NMR detection. (a) Experimental setup: tap water is thermally polarized by passing through a 1.4 kG permanent magnet before flowing into a 2.5 cm diameter cylinder located near the magnetometer inside magnetic shields. Pump and probe laser beams pass through evacuated glass tubes to avoid air turbulence. The K cell is a 3.8 cm dia. glass cylinder containing 2.5 atm of He gas and 60 torr of N_2 gas and a small droplet of K metal. (b) Single-shot NMR signal excited with a $\pi/2$ pulse and filtered with a bandwidth of 20 Hz. From the fit (dashed line) we determine $T_2^* = 1.7$ sec. (c) FFT of the NMR signal. The magnetic noise has a flat spectrum with a noise floor of 2×10^{-14} T/Hz $^{1/2}$.

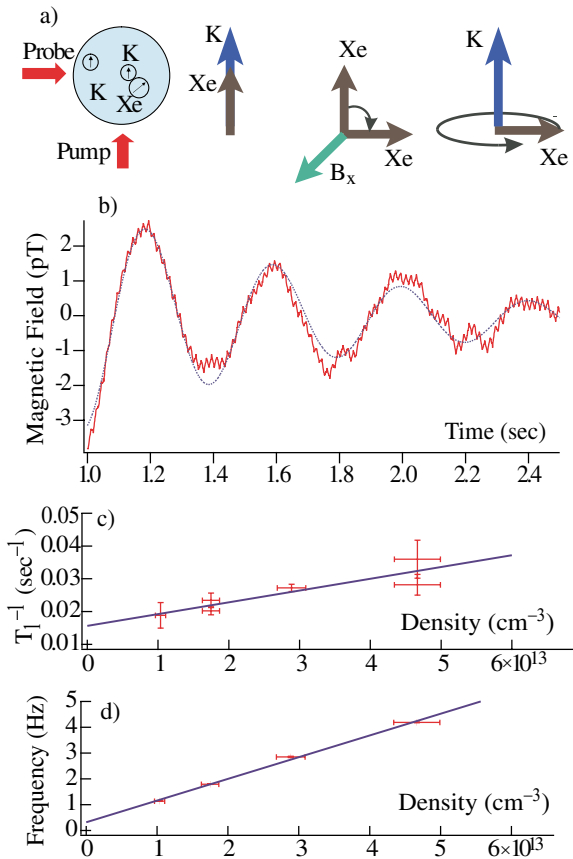


FIG. 2 (color online). Detection of ^{129}Xe NMR signal. (a) Schematic of the experiment and 3 steps of signal detection: polarization of ^{129}Xe by spin exchange, tipping of ^{129}Xe spins with a constant field, and precession of ^{129}Xe spins around the K magnetization. (b) A single ^{129}Xe spin-precession signal following the tipping pulse at $t = 0$ with a fit (dashed line). From the fit, the initial amplitude of the signal at $t = 0$ is 11.4 pT, the frequency is 2.46 Hz, and the transverse relaxation time $T_2^* = 0.78$ sec. (c) Measurement of T_1 as a function of K density. The slope of the fit gives the K-Xe spin-exchange rate $\sigma_{\text{SE}}\bar{v} = 3.6(9) \times 10^{-16} \text{ s}^{-1} \text{ cm}^{-3}$ and the intercept gives the wall relaxation rate $T_{\text{wall}}^{-1} = 0.016(3) \text{ s}^{-1}$. (d) The ^{129}Xe spin-precession frequency as a function of K density. The slope of the fit $8.4(3) \times 10^{-14} \text{ Hz/cm}^3$ is proportional to κ_0 .

oscillation with a small second-order polynomial correction for a background drift. The transverse spin relaxation time T_2^* is determined by the inhomogeneities of the K polarization across the cell. We found that applying a B_z field of 10–100 μG and increasing the optical pumping rate increases the ^{129}Xe signal by creating a higher and more uniform K polarization but lowers the intrinsic magnetometer sensitivity. This compromise can be avoided by separating the regions of polarization and detection of ^{129}Xe atoms.

By measuring the equilibrium ^{129}Xe signal from a train of $\pi/2$ pulses as a function of the separation time between the pulses we determined T_1 relaxation time of ^{129}Xe for different temperatures corresponding to different densities

of K. Measurements of the effects of K-K spin-exchange collisions [6,25] on the K Larmor resonance frequency and linewidth were used to determine the density and the polarization of K atoms. For example, at 180°C the potassium polarization is $P_K = 85\%$ and the density is $[K] = 2.9 \times 10^{13} \text{ cm}^{-3}$, about 3 times smaller than saturated vapor pressure. The dependence of $1/T_1$ on the density of K is shown in Fig. 2(c) from which we determined the K- ^{129}Xe spin-exchange cross section, $\sigma_{\text{SE}} = 6.3 \times 10^{-21} \text{ cm}^2$, which compares well with a theoretical estimate $\sigma_{\text{SE}} = 8 \times 10^{-21} \text{ cm}^2$ [24]. We also measured the Xe precession frequency as a function of K density, as shown in Fig. 2(d). In accordance with Eq. (2) the frequency is proportional to the density of K atoms. From the slope of the fit we determined $\kappa_0 = 540$, in good agreement with $\kappa_0 = 660$ calculated in [24].

The equilibrium ^{129}Xe polarization is given by $P_{\text{Xe}} = P_K \sigma_{\text{SE}} \bar{v} [K] / (T_{\text{wall}}^{-1} + \sigma_{\text{SE}} \bar{v} [K])$ and is equal to approximately 35% at 180°C. For the ^{129}Xe density of $2 \times 10^{13} \text{ cm}^{-3}$ the effective field seen by K atoms is $B_K = 12$ pT, in excellent agreement with the measured signal of 11.4 pT after correcting for the signal decay during the dead time of the magnetometer. The S/N is approximately equal to 10 in a bandwidth of 10 Hz, and the effective measurement volume determined by the intersection of the pump and probe beams is about 1 cm^3 . Thus, the magnetometer sensitivity is about $7 \times 10^{11} / \text{Hz}^{1/2}$ ^{129}Xe atoms. This detection technique can be easily adapted for detection of low ^{129}Xe concentration in a flow-through system [26] as long as ^{129}Xe spends much less than $T_1 \sim 20$ sec in the cell. ^{129}Xe can be initially polarized by optical pumping, flow through the sample where the information is encoded in the longitudinal polarization [16], and then flow through the K cell for detection. In a dedicated spin-detection cell it should be possible to achieve magnetic field sensitivity of better than $1 \text{ fT/Hz}^{1/2}$ [7], giving sensitivity of about 10^9 ^{129}Xe spins in a single shot.

Atomic magnetometers are also unique in allowing simple construction of multichannel systems. The electronics needed for each channel is much simpler than for an rf pickup coil or a SQUID detector and there is no inductive coupling between different channels. Parallel MRI techniques using phased rf arrays have been used to reduce imaging time by omitting some phase-encoding steps in a traditional MRI sequence [27]. It is well known that even a complete knowledge of the magnetic field outside of a closed volume is not sufficient to reconstruct the distribution of an arbitrary static current or magnetization inside the volume. The situation is different in NMR, where the magnetization starts out parallel to the magnetic field and always has a nonzero net magnetic moment, eliminating possible silent sources. However, the information obtained from the external fields is still insufficient for imaging. For example, a sphere with a uniform magnetization produces a pure magnetic dipole field, which has a degeneracy

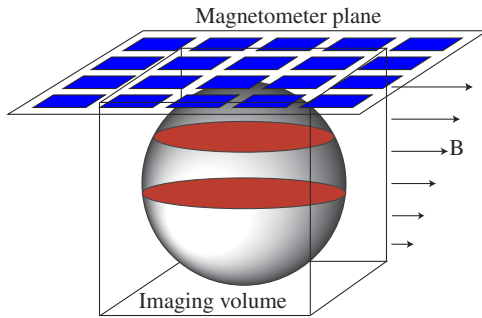


FIG. 3 (color online). Schematic of an MRI technique using a planar array of magnetometers. The ambiguity in the size of a spherical magnetization distribution is removed by applying a linear gradient that separates the object into slices in the frequency domain.

between the magnetization and the radius of the sphere. As a result, inversion procedures using a 3D grid of discrete dipoles [28,29] are not unique. It can be shown that at least one magnetic field gradient has to be applied to solve the inverse problem uniquely. The magnetic field gradient separates different slices of the sample in frequency, and within each slice an image can be uniquely obtained from the array of sensors, as illustrated in Fig. 3. This problem is analogous to the determination of a two-dimensional current density or susceptibility distribution using magnetic field measurements [30–32]. The inverse problem can be solved exactly. However, the spatial resolution drops exponentially with the distance between the magnetometer plane and the imaging slice, limiting the spatial resolution depending on the available S/N . With adequate S/N , a 3D image can be obtained from a single FID in a time on the order of 1 msec, set by the maximum bandwidth of the atomic magnetometer.

In conclusion, we have demonstrated detection of proton and xenon NMR signals with an atomic magnetometer and discussed possible unique applications of this detection technique for ultrasensitive detection of noble gas NMR and multichannel MRI imaging.

This work was supported by NSF, Packard Foundation, and Princeton University.

-
- [1] R. McDermott, A.H. Trabesinger, M. Muck, E.L. Hahn, A. Pines, and J. Clarke, *Science* **295**, 2247 (2002).
 [2] Ya. S. Greenberg, *Rev. Mod. Phys.* **70**, 175 (1998).
 [3] D.M. TonThat, M. Ziegeweid, Y.Q. Song, E.J. Munson, S. Appelt, A. Pines, and J. Clarke, *Chem. Phys. Lett.* **272**, 245 (1997).
 [4] J.J. Heckman, M.P. Ledbetter, and M.V. Romalis, *Phys. Rev. Lett.* **91**, 067601 (2003).

- [5] D. Budker, W. Gawlik, D.F. Kimball, S.M. Rochester, V.V. Yashchuk, and A. Weis, *Rev. Mod. Phys.* **74**, 1153 (2002).
 [6] J.C. Allred, R.N. Lyman, T.W. Kornack, and M.V. Romalis, *Phys. Rev. Lett.* **89**, 130801 (2002).
 [7] I.K. Kominis, T.W. Kornack, J.C. Allred, and M.V. Romalis, *Nature (London)* **422**, 596 (2003).
 [8] C. Cohen-Tannoudji, J. DuPont-Roc, S. Haroche, and F. Laloë, *Phys. Rev. Lett.* **22**, 758 (1969).
 [9] N.R. Newbury, A.S. Barton, P. Bogorad, G.D. Cates, M. Gatzke, H. Mabuchi, and B. Saam, *Phys. Rev. A* **48**, 558 (1993).
 [10] V.V. Yashchuk, J. Granwehr, D.F. Kimball, S.M. Rochester, A.H. Trabesinger, J.T. Urban, D. Budker, and A. Pines, *Phys. Rev. Lett.* **93**, 160801 (2004).
 [11] B.C. Grover, *Phys. Rev. Lett.* **40**, 391 (1978).
 [12] S.R. Schaefer, G.D. Cates, T.R. Chien, D. Gonatas, W. Happer, and T.G. Walker, *Phys. Rev. A* **39**, 5613 (1989).
 [13] M.S. Albert, G.D. Cates, B. Driehuys, W. Happer, B. Saam, C.S. Springer, and A. Wishnia, *Nature (London)* **370**, 199 (1994).
 [14] M.M. Spence, S.M. Rubin, I.E. Dimitrov, R.J. Ruiz, D.E. Wemmer, A. Pines, S.Q. Yao, F. Tian, and P.G. Schultz, *Proc. Natl. Acad. Sci. U.S.A.* **98**, 10654 (2001).
 [15] A. Cherubini and A. Bifone, *Prog. Nucl. Magn. Reson. Spectrosc.* **42**, 1 (2003).
 [16] A.J. Moule, M.M. Spence, S.I. Han, J.A. Seeley, K.L. Pierce, S. Saxena, and A. Pines, *Proc. Natl. Acad. Sci. U.S.A.* **100**, 9122 (2003).
 [17] H.J. Jänsch, P. Gerhard, M. Koch, and D. Stahl, *Chem. Phys. Lett.* **372**, 325 (2003).
 [18] K.R. Minard and R.A. Wind, *J. Magn. Reson.* **154**, 336 (2002).
 [19] L. Ciobanu, D.A. Seeber, and C.H. Pennington, *J. Magn. Reson.* **158**, 178 (2002).
 [20] S.R. Garner, S. Kuehn, J.M. Dawlaty, N.E. Jenkins, and J.A. Marohn, *Appl. Phys. Lett.* **84**, 5091 (2004).
 [21] W. Happer and H. Tang, *Phys. Rev. Lett.* **31**, 273 (1973).
 [22] T.W. Kornack and M.V. Romalis, *Phys. Rev. Lett.* **89**, 253002 (2002).
 [23] M.V. Romalis and G.D. Cates, *Phys. Rev. A* **58**, 3004 (1998).
 [24] T.G. Walker, *Phys. Rev. A* **40**, 4959 (1989).
 [25] I.M. Savukov and M.V. Romalis, *Phys. Rev. A* **71**, 023405 (2005).
 [26] B. Driehuys *et al.*, *Appl. Phys. Lett.* **69**, 1668 (1996).
 [27] R.M. Heidemann *et al.*, *European Radiology* **13**, 2323 (2003).
 [28] D. Kwiat, S. Einav, and G. Navon, *Med. Phys.* **18**, 251 (1991).
 [29] N.G. Sepulveda, I.M. Thomas, and J.P. Wikswo, *IEEE Trans. Magn.* **30**, 5062, (1994).
 [30] B.J. Roth, N.G. Sepulveda, and J.P. Wikswo, *J. Appl. Phys.* **65**, 361 (1989).
 [31] S. Tan, Y.P. Ma, I.M. Thomas, and J.P. Wikswo, *IEEE Trans. Magn.* **32**, 230 (1996).
 [32] D.J. Sheltraw and E.A. Coutsiyas, *J. Appl. Phys.* **94**, 5307 (2003).